Journal of Hazardous Materials 490 (2025) 137765

Contents lists available at ScienceDirect

Journal of Hazardous Materials

journal homepage: www.elsevier.com/locate/jhazmat

Removal of vanadium(V) ions from acidic water using reusable manganese oxide sorbents

Peirou Li [a,*], Laura Newsome [a], Arthur Graf [b], Karen A. Hudson-Edwards [a], David Morgan [b], Richard Crane [a]

[a] Camborne School of Mines and Environment and Sustainability Institute, University of Exeter, TR10 9FE, UK
[b] HarwellXPS, Research Complex at Harwell R92, Oxfordshire OX11 0FA, UK

HIGHLIGHTS

- Natural, synthetic and commercially-available MnOx were investigated for V removal.
- Natural MnOx has the highest adsorption capacity (54 mg V/g at pH 3).
- Highest amounts of V sorbed at pH < 3.
- MnOx can be regenerated and reused maintaining/enhancing V adsorption efficiency.

GRAPHICAL ABSTRACT

Adsorption of vanadium by MnOx and its regeneration for reuse.

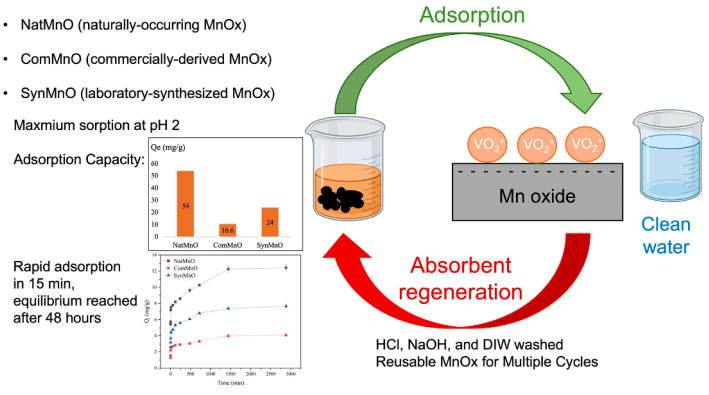

ARTICLE INFO

Keywords:
Manganese oxide
Vanadium adsorption
Kinetic models
Isotherm models
Regeneration
Surface chemistry
XPS

ABSTRACT

Manganese oxide (MnOx) was studied for its ability to adsorb vanadium (V) ions for applications in acidic water treatment. Three MnOx types: naturally-occurring (NatMnO), commercially-derived (ComMnO), and laboratory synthesised (SynMnO) were examined in batch systems under varying pH, adsorbent dosage, ionic strength, and contact time. The greatest V sorption occurred at acidic pH, following the order: NatMnO > SynMnO > ComMnO, with maximum adsorption capacities of 54.0, 26.0, and 10.4 mg/g, respectively (at pH 3.0, mass/volume ratio of 2 g/L, concentration of 100 mg/L, 24 hours). Adsorption equilibrium data best fit the Freundlich isotherm, indicating multilayer adsorption, while kinetic data followed a two-constant rate model, suggesting both physical and chemical sorption. Solution pH was found to have a significant impact, with V removal by MnOx most effective at low pH, likely due to the negative zeta potential of the MnOx under such conditions. MnOx reusability was investigated using repeated sorption and desorption experiments with 0.1 M HCl, 0.1 M NaOH, and deionised water to regenerate the MnOx. The regenerated MnOx exhibited similar or enhanced ability to sorb V ions from solution. Overall, these results confirm the unique ability of MnOx as a reusable sorbent for V removal from acidic water, while also enhancing our mechanistic understanding of the removal process. This

* Corresponding author.
E-mail address: pl476@exeter.ac.uk (P. Li).

https://doi.org/10.1016/j.jhazmat.2025.137765
Received 2 November 2024; Received in revised form 22 February 2025; Accepted 25 February 2025
Available online 25 February 2025

finding supports the development of sustainable solutions for acidic water treatment, contributing to efforts to address this critical environmental challenge.

1. Introduction

Vanadium (V) is a strategic metal essential to modern industry, including steelmaking, aerospace, automotive, bridges, and batteries [25,79,8]. Naturally, V occurs as oxides, sulfides, and phosphates, often associated with other metals like iron, titanium, lead, aluminium, zinc, and uranium, with iron and titanium deposits being the most significant [33,57,86]. Vanadium enters the environment from natural processes (e.g., rock leaching, vanadium-enriched slag, soil erosion, and dry deposition) and human activities (e.g., industrial processes, leaching of vanadium-enriched slag, urban sewage sludge, fertilizers, and mining operations) [67]. Exploitation of V resources has led to severe environmental issues, positioning V as an emerging contaminant, posing a growing risk to human and environmental health [39]. For instance, V concentrations in mining-affected water in the Mustavaara mine in northern Finland range between 6.5 and 99.1 mg/L [82]. Such elevated V concentrations often pose significant risks to both human and ecosystem health. For humans, the risks include asthma, rhinitis, general anemia, and an increased likelihood of uremia and lung cancer [75].

High levels of V, especially vanadium pentoxide (V_2O_5), pose substantial health risks. The International Agency for Research on Cancer (IARC) classifies V_2O_5 as a probable human carcinogen, and concentrations above 100 mg/L are neurotoxic to humans and animals [50,85]. Regulatory guidelines are also in place: the U.S. Environmental Protection Agency (EPA) has proposed a reference concentration of 21 μg/L for V, while China has set a limit of 50 μg/L for V in drinking water [68,73]. Given the stringently low concentration of these environmental quality standards it is vital that new water treatment technologies are developed to extract V from contaminated waters. An emerging issues, however, is that V is a widely used metal and occurs in a wide range of waste products and leachates [1,44,45,72]. For example, the production of one tonne of V_2O_5 product requires the consumption of 300 tonnes of water, which can become polluted with V [37]. The discharge of such wastewater can release considerable amounts of V into the environment. Given such activities are currently expanding worldwide, environmental and human health risks are accelerating [54,58,9].

To date, various techniques have been employed for V removal and separation, including solvent extraction [70], chemical precipitation [22], membrane techniques [52], and adsorption [11,34,36,71]. Amongst these routes adsorption has received considerable interest and numerous adsorbents, such as natural materials, clays, metal oxides or hydroxides, chitosan, and activated carbon, have been developed [71]. However, to date there have been few instances of commercially viable applications due to their low selectivity, low adsorption capacity, lengthy equilibration times, and excessive costs [6]. There is a strong consequent demand for further research into the development of new sorbents which are effective for V removal but also low cost, environmentally compatible and reusable.

In recent years manganese oxide/hydroxide minerals (MnOx) have gained attention for a wide range of water treatment applications due to their low cost, low toxicity, and ability to be regenerated and reused [53,77]. They also retains a net negative zeta potential (surface charge) even at relatively acidic pH conditions [16,81] which enables high efficacy for the removal of cations from acidic waters (such as acid rock drainage, or acidic processing wastes), for which other sorbents often prove ineffective [40,51,59]. For example, MnO_2 nanoflowers have been shown to be highly efficient in the oxidative degradation of organic dyes, with amorphous forms showing excellent rhodamine removal efficiency (99 %) within 10 minutes under acidic conditions [14]. Hydrated Mn oxide (HMO) synthesized by Hu et al. [24] demonstrated a high removal efficiency of Zr (IV) ups to 99.9 % (80 ppb) under optimal conditions. Wang et al. [69] reported that Sb (III) was rapidly and completely removed after a 10-minute reaction at different Sb (III)/-biogenic MnOx (BioMnO) molar ratios (97.8–100 %, under 787 ppb).

Despite the promising properties of MnOx and the widespread occurrence of V-bearing waters there have been few studies focusing on the sorption of V onto MnOx [2,3,84]. In addition, there is very little mechanistic information available on the adsorption behaviour of V on MnOx under acidic conditions, even though this is the most common geochemical condition of V-bearing water worldwide. This study has therefore been established to bridge this gap in our understanding and further investigate the adsorption mechanisms of V onto MnOx derived through different routes: naturally-occurring MnOx (NatMnO), commercially-derived (ComMnO), and laboratory synthesised (hydrothermal method) MnOx (SynMnO). Such fundamental mechanistic insight is an essential first step towards development of new technology for the removal of V from the aqueous phase to both safeguard the environment but also provide new alternative V sources to build the circular economy.

2. Experimental design

2.1. Materials and chemicals

Potassium permanganate ($KMnO_4$, ≥99.0 %), manganese (II) chloride tetrahydrate ($MnCl_2{\cdot}4\ H_2O$), sodium chloride (NaCl, 99.5 %), sodium hydroxide (NaOH, 99.0 %), sodium metavanadate ($NaVO_3$, ≥99.9 %), sodium nitrate ($NaNO_3$, 98 +%), nitric acid (HNO_3, 70.0 %), and hydrochloric acid (HCl, 37.0 %) were purchased from Fisher Scientific UK Ltd. All reagents were of analytical grade, and solutions were prepared with deionized water.

This study utilized naturally-occurring MnOx (NatMnO), commercially-derived MnOx (ComMnO), and laboratory synthesised MnOx (SynMnO). To represent naturally-occurring MnOx minerals, a sample was obtained from the British Geological Survey collection, taken from the summit area of Tropic Seamount in the northeast Atlantic in 2016. ComMnO was purchased from Fisher Scientific UK Ltd (Manganese(IV) oxide, 99 %, 10 mesh, CAS 1313–13–9). SynMnO was synthesized using a modified hydrothermal method from Tebo et al. [65]. Briefly, filter-sterilized solutions were prepared with deionized water: 18.8 g $MnCl_2{\cdot}4\ H_2O$ in 320 mL, 10.0 g $KMnO_4$ in 320 mL, 7.0 g NaOH in 360 mL, 1.0 M NaCl (pH 10), 0.01 M NaCl (pH 10). The $KMnO_4$ solution was added to the NaOH solution over 5 minutes while stirring. The $MnCl_2$ solution was then added to the $KMnO_4$ solution over 35 minutes while stirring, forming a black MnOx precipitate. The precipitate was allowed to settle, the supernatant discarded, and the mixture centrifuged by centrifugation (Avanti JE Rotor JS 5.3, Beckman Coulter, USA) at 5500 rpm for 20 minutes at room temperature. The supernatant was discarded again, and the precipitate resuspend in 1 M NaCl and shaken for 1 hour at 180 rpm. This step was repeated five times using 0.01 M NaCl, leaving the suspended oxides to shake 12 hours (180 rpm). The final product was washed with deionised water three times and dried in an oven at 100 °C. All MnOx were ground with a Tema Mill Unit with ring mill (tungsten carbide, diameter: 16 cm, wight: 12 kg, Siebtechnick, Germany) and sieved under 75 μm for V adsorption experiments.

2.2. Experimental design

2.2.1. Adsorption experiments

Adsorption experiments were conducted to identify the optimum conditions for V sorption to MnOx. Different MnOx dosage (2, 4, 8, 16 g/L) and initial pH values (2, 3, 4, 5, 6, 7, 8, and 9, generated by

adjustment with 1 M HNO_3 or 1 M NaOH as appropriate) were tested. Various ionic strengths (0.001, 0.005, 0.01, 0.02, 0.05, and 0.1 M) of anions (generated by addition of $NaNO_3$) were also investigated. Experimental solutions were prepared with the addition of V as $NaVO_3$ (100 mg/L V). All experiments were performed in 50 mL falcon tubes with constant shaking at 180 rpm and at room temperature (20 ± 1 °C).

The adsorption efficiency of V(V) (E (%)) was determined by using the following equation:

$$E(\%) = \frac{C_0 - C_e}{C_0} \times 100\% \quad (1)$$

The equilibrium adsorption capacity was determined using the equation:

$$Q_e = \frac{C_0 - C_e}{m} \times V \quad (2)$$

where Q_e is the equilibrium amount of V(V) adsorbed per unit mass of adsorbent (mg/g), m is the sorbent mass (g), V is the volume of solution (L), C_e is the equilibrium concentration (mg/L) and C_0 is the initial concentration (mg/L).

2.2.2. Kinetic adsorption experiments

Kinetic adsorption experiments were used to determine possible adsorption mechanisms. 2 g/L of MnOx was added to 100 mg/L V solution (50 mL, pH = 3.0, 0.01 M $NaNO_3$) then measured at various times (1, 2, 5, 15, 60, 120, 240, 480, 720, 1440, 2880 min). To predict the adsorption rates, pseudo-first order (PFO) [32], pseudo-second order (PSO) [12], two-constant rate model [49], Elovich [41], and intra-particle diffusion (IPD) models were used to fit the experimental data. More details are described in the Supporting Information (SI) (Text S1).

2.2.3. Adsorption isotherms experiment

The adsorption isotherm experiment was used to investigate the adsorption performance of three MnOx. 2 g/L of MnOx was added to initial V concentrations range from 10, 20, 40, 100, 200, 400, 800, and 1000 mg/L diluted from a 1000 mg/L V stock solution (50 mL, pH = 3.0, 0.01 M $NaNO_3$) with an equilibrium time of 24 hours. To predict the adsorption behaviour of adsorbate on the adsorbent surface, five theoretical isotherm models (Langmuir, Freundlich, Temkin, Dubinin-Radushkevich (D-R), and Redlich–Peterson (R-P)) were used to fit the experimental data. Adsorption isotherms models' details are described in SI Text S2.

2.2.4. Adsorption–desorption experiments

To evaluate the stability of MnOx, adsorption–desorption experiments were conducted. After V adsorption (as per the kinetics adsorption experiment above), the mixture was centrifuged (5500 *g*, 8 min) and washed with DIW. The supernatant was then discarded and the MnOx was added to deionized water (DIW) for 24 hours of stirring to desorb the V.

To evaluate the reusability of MnOx, 50 mL 0.1 M HCl, 0.1 M NaOH, or DIW were added to the V-sorbed MnOx for 24 hours of stirring. The mixture was centrifuged and washed with DIW again after 24 h. The supernatant was discarded and the precipitate was dried at 30 °C for 24 hours. The process was repeated for three cycles of adsorption–desorption. Both adsorption and desorption experiments were conducted under identical conditions (20 ± 1°C, pH = 3.0, 0.01 M $NaNO_3$,100 mg/L V 2 g/L MnOx,).

At the cessation of each sorption or desorption experiment the sorbent and supernatant were isolated by centrifugation (5500 *g* for 8 min, Megafuge ST Plus Series, Thermo Fisher Scientific, Germany). The supernatant was extracted using a syringe, passed through a 0.45 μm filter, and then diluted into 2 % HNO_3 for V analysis using Inductively Coupled Plasma Optical Emission Spectrometry (ICP-OES, Agilent 5110 Series, USA) [38]. The sorbent was extracted, washed, and dried for further characterization. All sorption or desorption experiments were performed in triplicate, and a 100 mg/L V solution with no MnOx added was used as a control.

pH value was measured with a Fisher brand FB68801 Semi-Micro pH meter (UK).

2.3. Characterization of MnOx

To compare the physical properties of three MnOx, crystalline mineral phases were identified using a monochromatic Cu-Kα radiation (λ = 0.154 nm) X-ray powder diffractometer (XRD, D8 advanced, Bruker, German) at a scanning rate (2θ) of 4°/min. Images of the samples were obtained using a scanning electron microscope (SEM, FEI Quanta FEG 650, Bruker, German) and transmission electron microscopy (TEM, JEM 1400, JEOL, Japan) with energy dispersive spectrometry (EDS) were used to visualize surface morphology and structure of adsorbents before and after adsorption of V. To obtain the specific surface area, pore volume, and pore size distribution of the MnOx, the samples were assessed using the nitrogen adsorption–desorption isotherm method with a Brunauer-Emmett-Teller Surface-Area Analyzer (BET, NOVA-Touch LX2, Anton Paar, USA). Samples were degassed at 40 °C for 19 hours before analysis. Surface zeta potentials (ζ) of the materials were measured at different pH using a zeta potential analyser (ZETASIZER NANO Z, Malvern Panalytical, UK).

To determine surface chemistry changes on the mineral, X-ray photoelectron spectroscopy (XPS) analysis was performed using a Thermo NEXSA XPS (Thermo Fisher Scientific, USA) fitted with a microfocussed monochromated Al kα X-ray source (1486.6 eV), spherical sector analyser, and 128 channel delay line detector. The powdered samples were mounted and pressed in a glass support and analysis was conducted roughly at the middle of the powder. Survey scans were recorded at a pass energy of 200 eV, and high-resolution scans recorded at 40 eV. Charge compensation was achieved using a dual-beam low-energy electron/ion source (Thermo Scientific FG-03, USA), operating at a background argon pressure below 10^{-7} Torr. Data was using CasaXPS v2.3.26PR1.0 [17] using Scofield sensitivity factors and an energy dependence of the kinetic energy raised to –0.6 as recommended by the instrument manufacturer. Where required, peak fitting was achieved using a Voigt type function characterised in CasaXPS by LA (1.53, 243), after removal of a Shirly background.

2.4. Statistical analysis

Data were presented as mean ± standard deviation and plotted using the Origin 2021 (OriginLab, USA). Statistical significance was analysed using one-way analysis of variance by using the SPSS 26.0 (International Business Machines Corporation, USA) with differences considered statistically significant at $p < 0.05$.

3. Results and discussion

3.1. Characterization of the adsorbents

3.1.1. XRD analysis

To determine the mineral phase of the MnOx used in this study, powder X-ray diffraction (XRD) was performed in the 2θ range of 10 – 80°. The XRD pattern of ComMnO (Fig. 1) showed diffraction peaks at 2θ values of 28.6°, 37.3°, 40.9°, 42.8°, 46.1°, 56.7°, 59.3° and 64.9°, corresponding to the rutile structure of β-MnO_2 tetragonal phase (COD Card 96–151–4111). No peaks related to other types of MnO_2 or amorphous MnO_2 were observed, indicating ComMnO is comprised of high purity and crystalline β-MnO_2. For NatMnO, low intensity and broad diffraction peaks at 26.7°, 37.0° and 67.5° were observed, and for SynMnO at 37.0° and 67.5°, both characteristic of hexagonal randomly stacked and single phased birnessite-type of δ-MnO_2 (ICDD Card 00–042–1316),

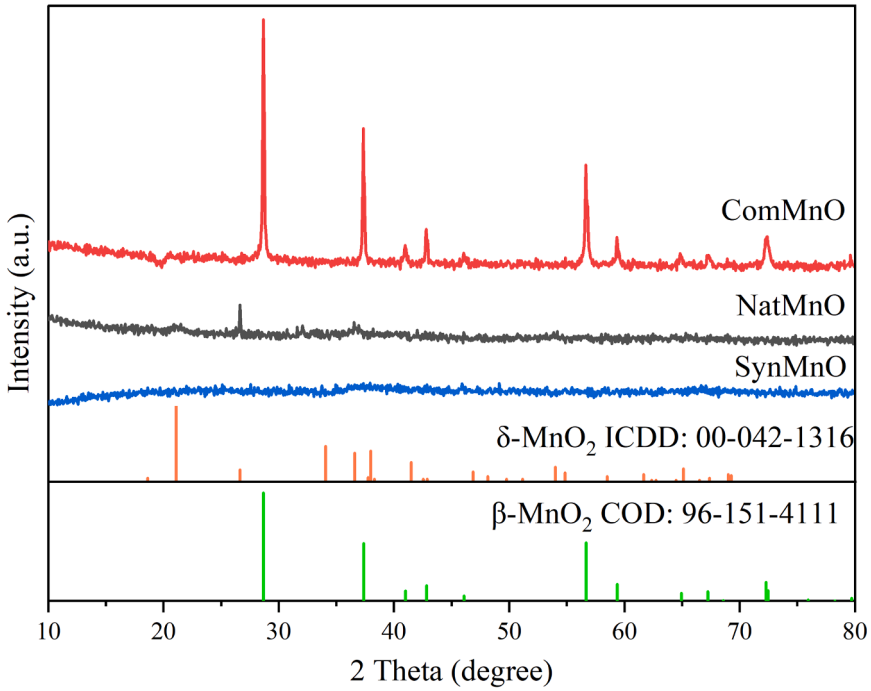

Fig. 1. XRD profiles of natural (NatMnO, black), commercial (ComMnO, red), and synthetic (SynMnO, blue) MnOx.

similar to the results of others [46,80]. The largely amorphous structure of NatMnO and SynMnO also indicates that they are likely to exhibit larger sorption capacity (per unit mass basis) than their crystalline polymorph [28].

3.1.2. *SEM and TEM images*

The structure of the MnOx was visualised by SEM and TEM (Fig. 2). NatMnO showed a layered morphology (Fig. 2a). However, the structure was irregular and significant particle agglomeration (clusters were 200 nm in diameter on average) was observed. SynMnO exhibited nanoscale particle clusters of average diameter 300 nm with uneven distribution, similar to those synthesised by others [46,74,80]. ComMnO particles were more regularly-shaped, exhibiting a higher degree of crystallinity but significant agglomeration (clusters were 1000 nm in diameter on average). Using a high-resolution TEM image of NatMnO, the intraplanar spacing was measured to be 2.8 Å (Fig. 2d), corresponding to the (201) planes of δ-MnO_2. For ComMnO, the interplanar fringe distance was 3.5 Å (Fig. 2h), corresponding to the (110) planes of β-MnO_2. For SynMnO, the interplanar fringe distance was 5.1 Å (Fig. 2l), corresponding to the (200) planes of δ-MnO_2.

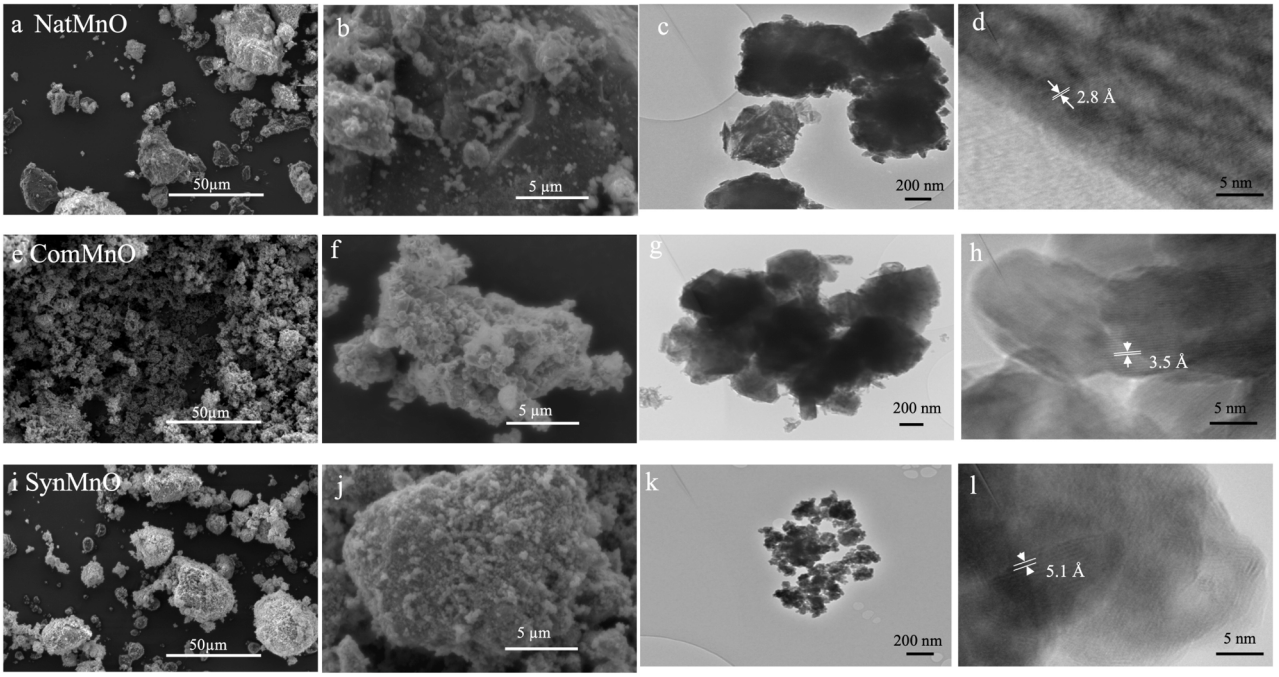

Fig. 2. SEM and TEM images of MnOx. (NatMnO (a-d), ComMnO (e-h), SynMnO (i-l), SEM (a, b, e, f, i, j), TEM (c, d, g, h, k, l)).

3.1.3. BET

NatMnO had a BET specific surface area of 35 m^2/g, a pore volume of 0.29 cm^3/g, and a pore size of 1.06 nm. ComMnO had a BET specific surface area of 3 m^2/g, a pore volume of 0.04 cm^3/g, and a pore size of 1.08 nm. SynMnO had a BET specific surface area of 27 m^2/g, a pore volume of 0.25 cm^3/g, and a pore size of 2.45 nm. Since 'mesoporous material' refers to solids based on ordered or disordered networks with either wide or narrow pore distributions ranging from 2 nm to 50 nm, SynMnO can also be considered a mesoporous material [64]. The BET surface areas of NatMnO and SynMnO were similar, and significantly higher than that of ComMnO. Furthermore, the total pore volume of NatMnO (0.29 cm^3/g) was larger than those of SynMnO (0.25 cm^3/g) and ComMnO (0.04 cm^3/g). According our XRD and SEM results, NatMnO and SynMnO both were characteristic of hexagonal randomly stacked and single phased birnessite-type of δ-MnO_2, which results a similar pore volume. And for ComMnO was observed corresponding to the rutile structure of β-MnO_2 tetragonal phase that has a more compact interatomic arrangement than δ-MnO_2, resulting in a smaller pore volume. NatMnO has the largest specific surface area (35 m^2/g) and the largest porosity (0.29 cm^3/g), providing more active sites for adsorption, and the larger pore volume allows for easier access and accommodation of adsorbent molecules, suggesting more favourable and efficient adsorption properties. A detailed description of the nitrogen isotherm adsorption/desorption for MnOx were included in SI Text S3 and Figure S1.

3.1.4. Zeta potential

The surface properties of MnOx can be expressed in terms of zeta potential. The zeta potentials of the MnOx as a function of solution pH are shown in Fig. 3. The point of zero charge (pH_{pzc}) of NatMnO, ComMnO, and SynMnO were determined to be 1.8, 4.6 and 1.6, respectively. Below the pH_{pzc}, the surface of MnOx exhibits a positive charge, promoting the uptake of anionic V species. These values are similar to others reported for MnOx. For example, the pH_{pzc} of synthetic MnOx synthesized by [81] were all below pH 3. Additionally, the pH_{pzc} of birnessite was reported to be 2.7 [16].

NatMnO and SynMnO consist of amorphous δ-MnO_2 (Fig. 1) suggesting that contaminants will have relatively easy access to reactive sites within the particle structure [23]. All MnOx are nanoscale, so they may have a high affinity for sorbing metal ions from solution [4]. Using the TEM and the BET data, it is hypothesised that NatMnO has the greatest potential for sorption due to the smallest particle size and the highest surface area.

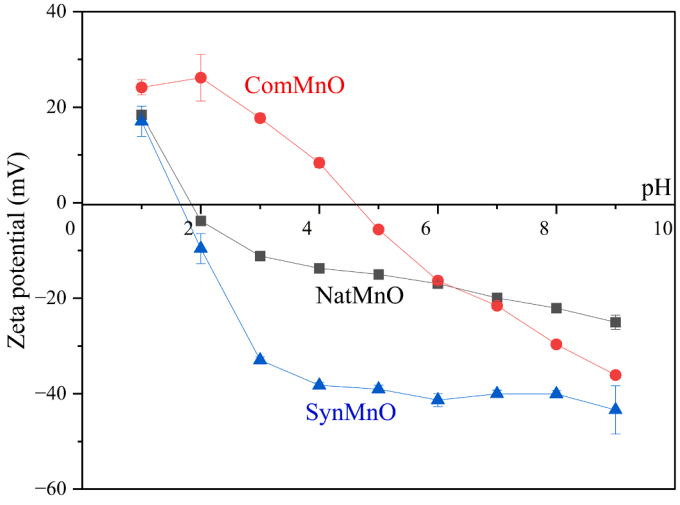

Fig. 3. Zeta potential of MnOx as a function of pH.

3.2. Optimal conditions for V sorption

3.2.1. Effect of pH on V adsorption

The effectiveness of V adsorption onto MnOx was generally highest at pH 2 (Q_e: NatMnO=17.1 mg/g, SynMnO=13.6 mg/g, ComMnO=2.37 mg/g). This effectiveness declined as the solution pH increased to 5, then increased between pH 5 and 7, and then slightly decreased from pH 7–9 (Fig. 4a).

Variations in pH impact the degree of ionization of the functional groups, the charge of adsorbent surface, and the prevailing species of metal ions, consequently affecting metal ion removal [71]. Vanadium exists as cationic VO_2^+, $VO(OH)_3$ and V_2O_5 in strongly acidic environments, and to various mono- or polynuclear anionic species ($VO_2(OH)_2^-$, $VO_3(OH)^{2-}$, $H_2V_2O_7^{2-}$, $HV_2O_7^{3-}$, VO_4^{3-}, $H_3V_{10}O_{28}^{3-}$, $H_2V_{10}O_{28}^{4-}$, $HV_{10}O_{28}^{5-}$, $V_{10}O_{28}^{6-}$, $V_2O_6(OH)^{3-}$, $V_2O_7^{4-}$, $V_3O_9^{3-}$, $V_4O_{12}^{4-}$) which occur in slightly acidic, neutral, or alkaline solutions [31]. The diagram of these oxidation states and major species of V with pH and redox potential is shown in Figure S2 [26].

In our study of V adsorption, NatMnO and SynMnO exhibited better adsorption performance because that their surfaces carried negative charge due to their lower pH_{pzc}, favouring the uptake of cationic VO_2^+ species at pH 2. As pH increased (2−5), the fraction of VO_2^+ decreased whereas the fraction of anionic species increased. In contrast, at pH 2–4, ComMnO was positively charged, leading to electrostatic repulsion with cationic VO_2^+, resulting in significantly lower adsorption efficiency compared to NatMnO and SynMnO. When pH was higher than 5, the surface of all three MnOx became negatively charged. Simultaneously, vanadium in solution primarily existed as anionic $H_3V_2O_7^-$, $H_2VO_4^-$, HVO_4^{2-} species, creating electrostatic repulsion with MnOx [48]. In the pH range of 7–10, the decline in V adsorption capacity was associated with competition between OH^- ions and the high-valence V oxyanions [48,61]. The uptake of vanadate on MnOx can potentially occur via an anion exchange mechanism, which involves the formation of a binuclear-bridged complex [47]. Considering that the actual wastewater pH concentration ranges from 2 to 3, further experiments were carried out at pH= 3 to investigate other factors.

3.2.2. Effect of ionic strength

To investigate the influence of ionic strength on V adsorption onto MnOx, a supporting electrolyte ($NaNO_3$, 0.001–0.1 M) was added to the V-bearing solutions (Fig. 4b). The adsorption of V on all MnOx exhibited a positive relationship with increasing ionic strength from 0.001 to 0.01 M, but then had a negative relationship from 0.01 to 0.1 M.

When electrostatic attraction plays an important role in metal cation removal, adsorption becomes sensitive to changes in ionic strength [43]. The lower concentrations of $NaNO_3$ (0.001–0.01 M) enhanced electrostatic attraction, promoting better electrostatic adsorption of V on MnOx. On the contrary, the highest concentration of $NaNO_3$ (0.1 M) likely reduced electrostatic adsorption, due to competition of excess Na^+ ions with V ions for adsorption sites on MnOx, thus affecting the physical adsorption capacity for V. Similar observations have previously been reported for V adsorption onto kaolinite [83] and red mud modified saw dust biochar [19], suggesting that Na^+ ions act as bridges, facilitating V adsorption. According to the surface chemistry theory proposed by Gouy Chapmann [21,43], when a solid adsorbent encounters sorbate species in the solution, it becomes enveloped by an electrical double layer, whose thickness notably expands in the presence of an electrolyte. This expansion hinders the proximity of adsorbent particles and metal species, resulting in a reduced uptake of V due to the decreased electrostatic attraction. The inhibiting effect of ionic strength may also be interpreted by (i) high concentration electrolyte ion (Na^+) competing with positively charged heavy metal ions for the same binding sites [18,42]; and (ii) ionic strength influencing the interfacial potential of metals, which in turn limits their transfer to the adsorbent surface [27].

Therefore, 0.01 M $NaNO_3$ was used in the solution to achieve optimal adsorption in subsequent experiments.

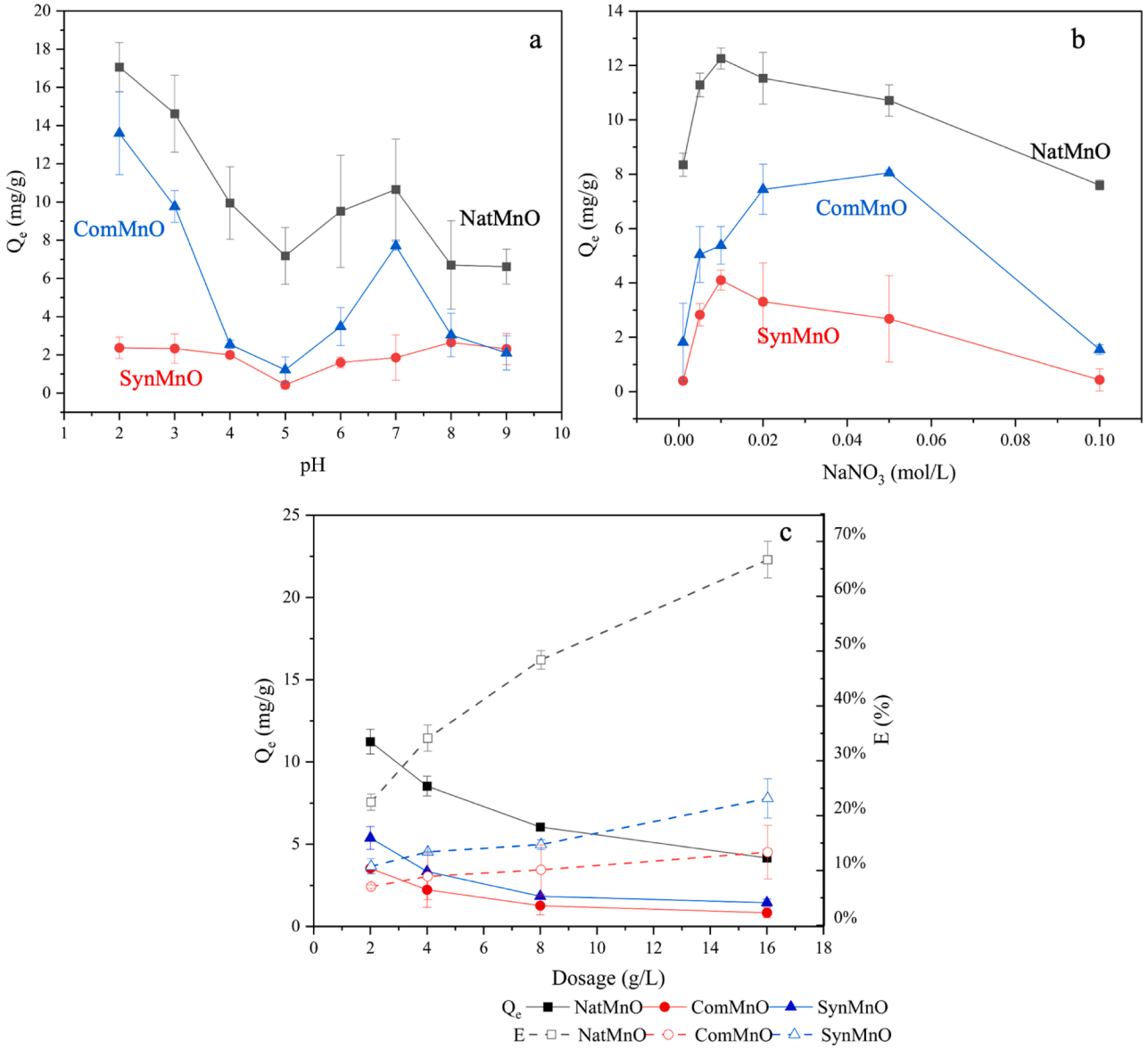

Fig. 4. Effects of pH (a), ionic strength (b), and dosages (c) on V removal by MnOx.

3.2.3. *Effects of adsorbent dosage*

For each MnOx, the removal efficiency (E (%)) increased and the adsorption capacity (Q_e) decreased with an increased dosage of MnOx (Fig. 4c). This effect may be due to the adsorption sites remaining unsaturated during the adsorption reaction as the adsorbent dosage increases, resulting in a decrease in adsorption capacity.

With the increase in the adsorbent dosage, the number of active adsorption sites in the unit volume of V solution increased, which leads to an increase in the adsorption efficiency. The largest amount of V adsorption was obtained by NatMnO with a dosage of 2 g/L (11.2 mg/g) and may be due to the largest surface area and pore volume.

Considering that the most favourable adsorption capacities towards V were at a dosage of 2 g/L, further experiments aimed at the determination of the kinetics and mechanism of adsorption were conducted at this concentration.

To investigate the relationship among pH, adsorbent dosages, ionic strength, and the removal of V, the Pearson's correlation test was used to analyse the correlations between these factors and adsorption capacity [60]. The results are shown in Table S4. There was a significant positive correlation ($p < 0.05$) between adsorbent dosage and V removal, and between reaction time and removal ($p < 0.01$) for all three types of Mn oxides. A significant negative correlation ($p < 0.05$) between pH and V removal was observed for NatMnO.

Overall, the maximum adsorption capacity of V occurred at 2 g/L MnOx dosing, with an optimal pH of 2 and an ionic strength of 0.01 M $NaNO_3$.

3.3. *Adsorption kinetics, isotherms and modelling*

3.3.1. *Adsorption kinetics*

The rate of V adsorption onto MnOx was high within the first 15 minutes, and then decreased slowly (60–720 min), approaching equilibrium over the next 24 hours and then no major further change was recorded after 48 hours (Fig. 5). Such rapid and efficient V sorption onto MnOx within 15 minutes highlights its significant potential as an advanced water treatment technology for V removal. The rapid initial adsorption can be attributed to the abundant availability of active sorption sites, extensive surface area, and mesoporous structure of MnOx [5]. However, as the sorption sites gradually became occupied, the sorption efficiency increased at a slower rate until equilibrium was

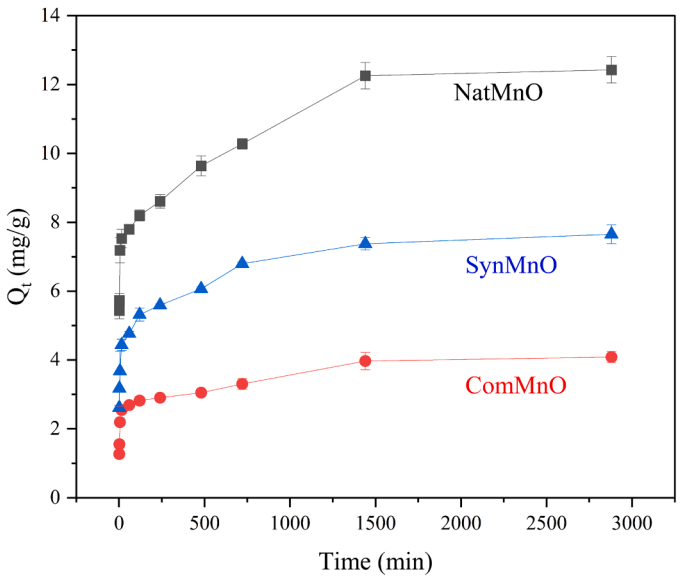

Fig. 5. V adsorption kinetics on MnOx.

reached, leaving residual V in solution. This likely occurred because the adsorption sites reached saturation, and repulsive forces from the adsorbed V prevented further V ion removal [18].

The experimental equilibrium adsorption capacities (Q_e) were 12.4 ± 0.38 mg/g (NatMnO), 4.09 ± 0.16 mg/g (ComMnO), and 7.65 ± 0.27 mg/g (SynMnO). The results of model fitting (Fig. 6) to predict the adsorption rates calculated Q_e values from the pseudo-first order (PFO) and pseudo-second order (PSO) model were 6.01 and 9.04 mg/g (NatMnO), 2.74 and 3.10 mg/g (ComMnO), and 4.81 and 6.08 mg/g (SynMnO), respectively. Analysis of R^2 for the fit of models showed that the adsorption of V by all three MnOx is good described by PSO (R^2>0.98, Fig. 6b, SI Table S1), as opposed to the weaker fit of the PFO model (R^2<0.87, Fig. 6a, SI Table S1). The Q_e values calculated from the PSO model were closer to the experimental equilibrium adsorption amounts. This demonstrates that the adsorption of V by MnOx followed PSO kinetics. The PFO equation only applied to the initial stage of the process; it showed a poor fit with the entire range of phase contact times [63]. The better fit of PSO model suggests the existence of more than one rate-controlling step [10]. This implies that the adsorption of V on MnOx may be influenced by chemisorption and valence forces, potentially occurring through the sharing or exchange of electrons [83].

The adsorption data of NatMnO and SynMnO also fit well with two-constant rate model (R^2>0.94), with a reasonable fit for ComMnO (R^2=0.87), suggesting that the adsorption process may involve chemical adsorption and complexation with active functional groups (e.g. C═O and -OH) or exchangeable H^+ ions (–C═O, and exchangeable Na^+) in the sorption process [42,76].

The fits of the Elovich model for all three MnOx were acceptable (R^2 > 0.89), suggesting that the adsorption process of V by these materials might be not a simple physical or chemical adsorption process, but rather a complex one controlled by diffusion (or mass transfer) processes and physisorption [35,62].

Q_t can be plotted against $t^{0.5}$, and if the result is a straight line through the origin it indicates that the adsorption process is completely controlled by intra-particle diffusion (IPD) [56]. By contrast, multi-linearity plots indicate that two or more steps influence the sorption process. The multi-linearity plots (Fig. 6e) suggest that V sorption onto MnOx was controlled by three reactions, consistent with the findings of others [15,29,55]. First, the fitted line deviated from the origin, indicating the involvement of both intraparticle and film diffusion in the rate-determining step [7]. According to value of the rate constant K_t (SI Table S1), the first stage (1–15 min) is the instantaneous sorption, occurring as rapid reactions attributed to film diffusion or macropore diffusion on the external sorption surfaces. NatMnO exhibited the fastest adsorption rate (K_{t-1}, SI Table S1). The abundance of

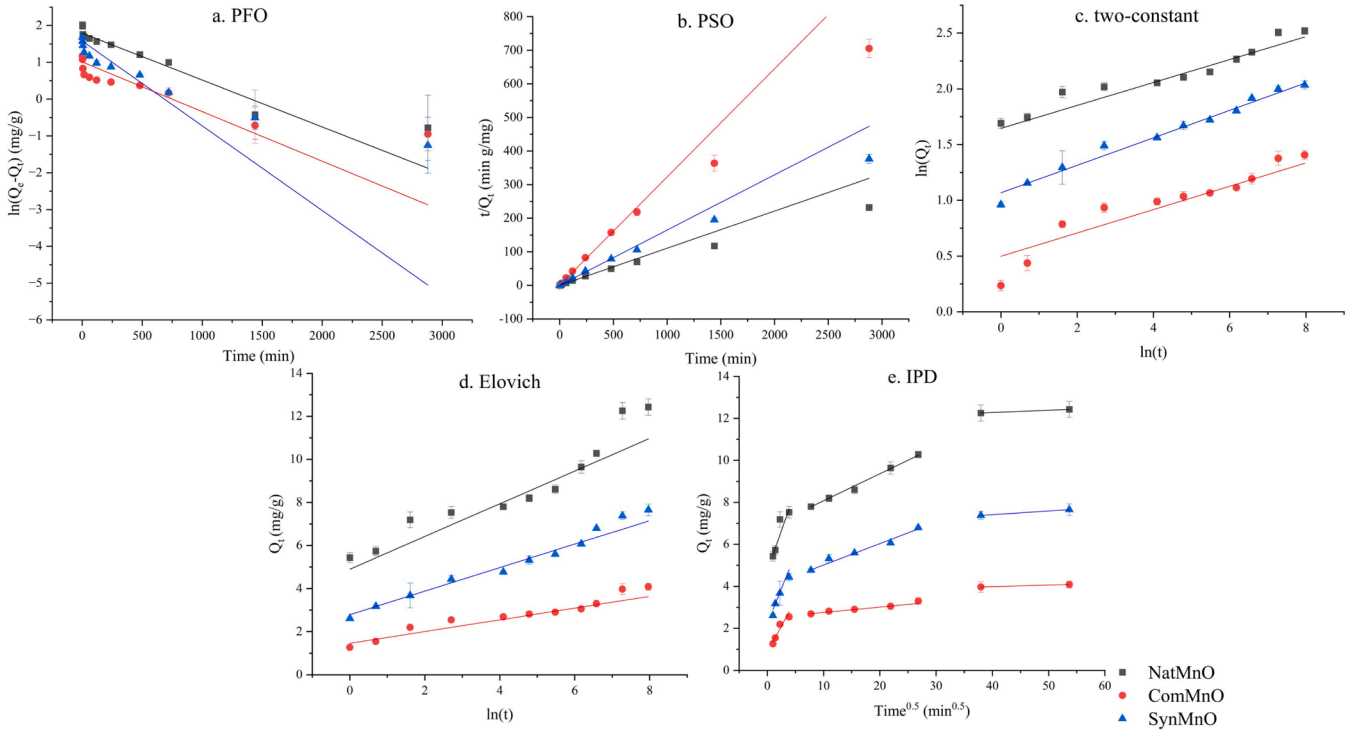

Fig. 6. V adsorption kinetics models on MnOx (a. pseudo-first order (PFO), b. pseudo-second order (PSO), c. two-constant, d. Elovich, e. intra-particle diffusion (IPD)).

sorption sites on the external surface of the MnOx and their strong interaction with V contributed to the rapid sorption rate observed during this stage. The second sorption stage (60–720 min) occurred on the interior surfaces, where particles likely diffused slowly into the micro- and mesopores of the adsorbent. During this stage, the adsorption amount of V on NatMnO and SynMnO were much higher than on ComMnO, which could be attributed to surface charge differences. During the third and final equilibrium stage (1440–2880 min), there was a gradual diffusion of V into micropores, leading to a reduced sorption rate due to the extremely low VO_2^+ concentration remaining in solution [15]. The intercept 'C' shows the boundary layer effect or surface adsorption of V, a higher C value implies a more significant contribution of surface adsorption in determining the rate (The order followed by NatMnO > SynMnO > ComMnO, SI Table S1) [78].

3.3.2. *Adsorption isotherms*

Adsorption isotherms provide qualitative information on the nature of the solute-surface interaction and describe the specific relationship between the concentration of adsorbate and its degree of accumulation onto adsorbent surface at constant temperature [30].

Considering the practical applications of the V(V) sorption process on MnOx, it was essential to determine the impact of the initial metal ion concentration on adsorption efficiency. Over 80 % V ions were removed from solutions containing 10 mg/L V by NatMnO and SynMnO (Fig. 7b). The increase in adsorption capacity at higher V concentrations is likely due to the stronger driving force between the adsorbent and sorbate at higher V ion concentrations [20].

Five theoretical isotherm models were used to fit the experimental data to predict the adsorption behaviour of adsorbate on the adsorbent surface (Fig. 8). For NatMnO, the Freundlich model exhibited the highest R^2 value (0.99, Fig. 8b, SI Table S2), indicating excellent compatibility with the experimental data. The Langmuir (Fig. 8a), Temkin (Fig. 8c), and Redlich–Peterson (Fig. 8e) models all had good linear fits ($R^2 > 0.96$, Table S2), suggesting a complex nature of the adsorption processes. The Langmuir model showed a good fit ($R^2 = 0.97$) with an R_L value of 0.63, indicating favourable adsorption of V on NatMnO, with sorption capacity of 54 mg V/g (Table S2). For ComMnO, experiment data were best fitted by Temkin model, followed by the Freundlich and Redlich–Peterson models, with poorer fits for the D-R and Langmuir models. This suggests that V adsorption on ComMnO was a multilayer process occurring on a non-uniform surface [13]. For SynMnO, the Redlich–Peterson isotherm exhibited the highest coefficient of determinations, like the Freundlich isotherm, indicating a better fit compared to those of the Langmuir and Temkin isotherms. The values of g (0.6002, SI Table S2) were not close to 1, suggesting that the isotherms approach the Freundlich rather than the Langmuir model.

According to the Langmuir model, the maximum V adsorption amounts were 54.0 mg/g by NatMnO (R^2=0.969, SI Table S2) and 26.0 mg/g by SynMnO (R^2=0.815, SI Table S2) which were numerically close to the experimental data (NatMnO: 46.7 mg/g, SynMnO: 29.8 mg/g). The Langmuir model did not fit ComMnO well and therefore cannot show a theoretical value for the maximum adsorption of ComMnO on V. The MnOx adsorbents were compared to previously published literature to determine their highest adsorption capacities for vanadium (SI Table S3). Compared with other adsorbent, the NatMnO and SynMnO in the present study showed a considerable high adsorption capacity of V (V) at low pH.

For all MnOx, the D-R model had lower R^2 values (< 0.87, Fig. 8c, SI Table S2). The poor fit of the D-R model may imply that the adsorption mechanisms for these MnOx are more complex and cannot be solely explained by this model. The values of the Freundlich parameter *1/n* (SI Table S2) were higher than 0 and n values (SI Table S2) were between 1 and 2 for all three MnOx, indicating favourable adsorption with moderate adsorption capacity.

3.4. *Mineral surface chemistry*

To determine the adsorption mechanism, characterization of the MnOx surfaces was carried out using SEM-EDS (SI Fig. S3). This analysis confirmed that V was present in all three MnOx, confirming that sorption had occurred. The morphology of MnOx after adsorption remained largely unchanged. The concentration of V adsorbed by MnOx (SI Table S5), determined using SEM-EDS, followed the same trend as the results obtained from ICP-OES: NatMnO exhibited a greater adsorption capacity for V than SynMnO and ComMnO.

XPS was undertaken to identify changes in Mn and V oxidation state upon the MnOx surface (Fig. 9). Carbon and oxygen spectra are provided in the Supplementary Information (SI Fig. S4). These data show that at the start of the experiment Mn was present as Mn(IV) in all three MnOx samples, and that no significant chemical change was recorded within residues following the use of MnOx for V adsorption. The Mn 2p spectra suggested the presence of mixed manganese oxidation states (Mn(II) and Mn(IV)), which remained consistent before and after exposure of the MnOx to the V-bearing solutions. The presence of V was confirmed by a

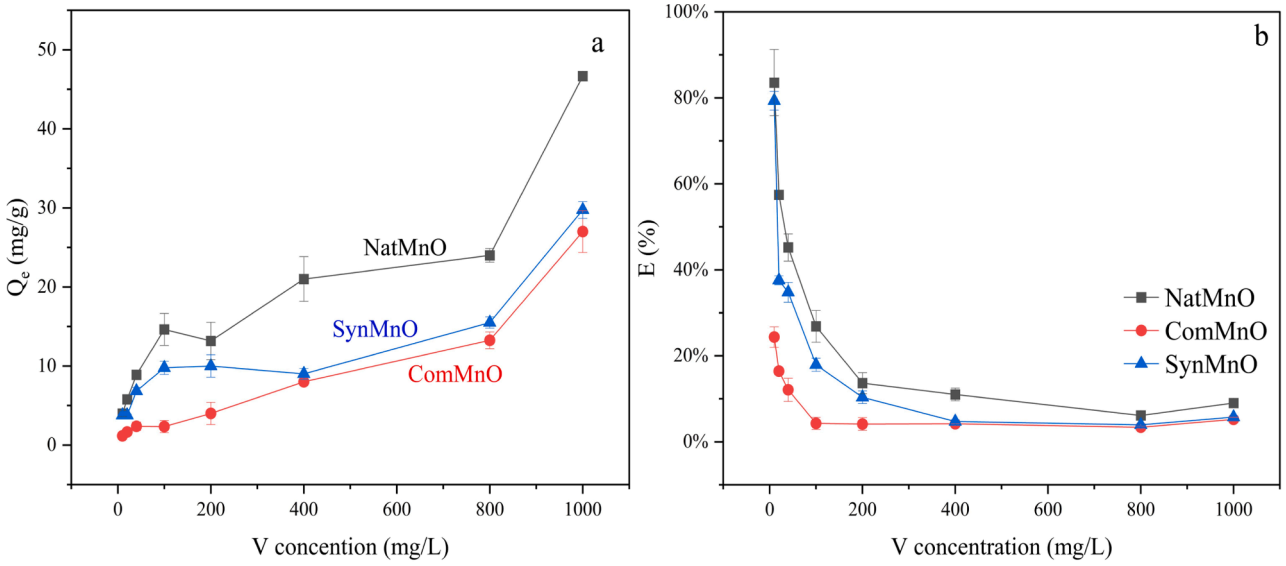

Fig. 7. Effects of initial V concentration on V removal by MnOx. (a. adsorption capacity, b. adsorption efficiency).

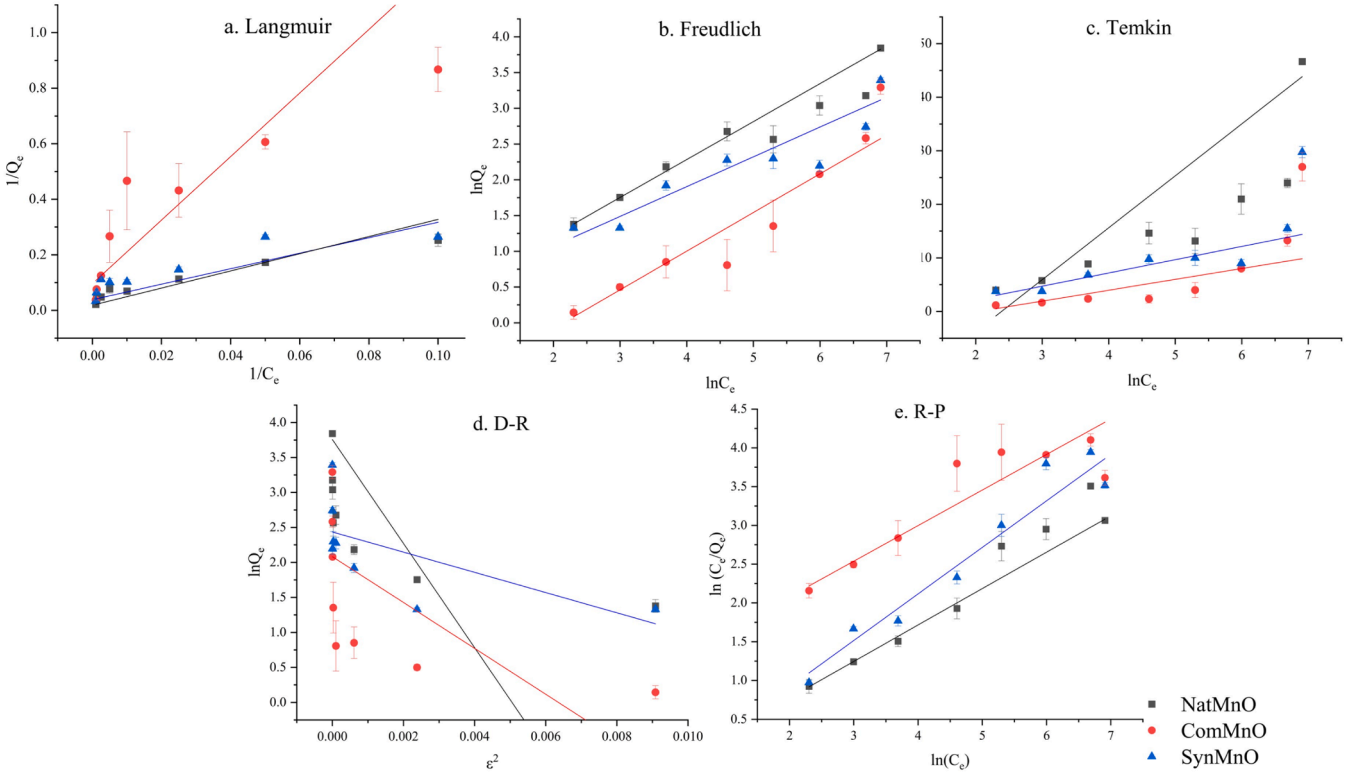

Fig. 8. V adsorption isotherm models on MnOx. (a. Langmuir model, b. Freundlich model, c. Temkin model, d. Dubinin-Radushkevich model (D-R), e. Redlich - Peterson model (R-P)).

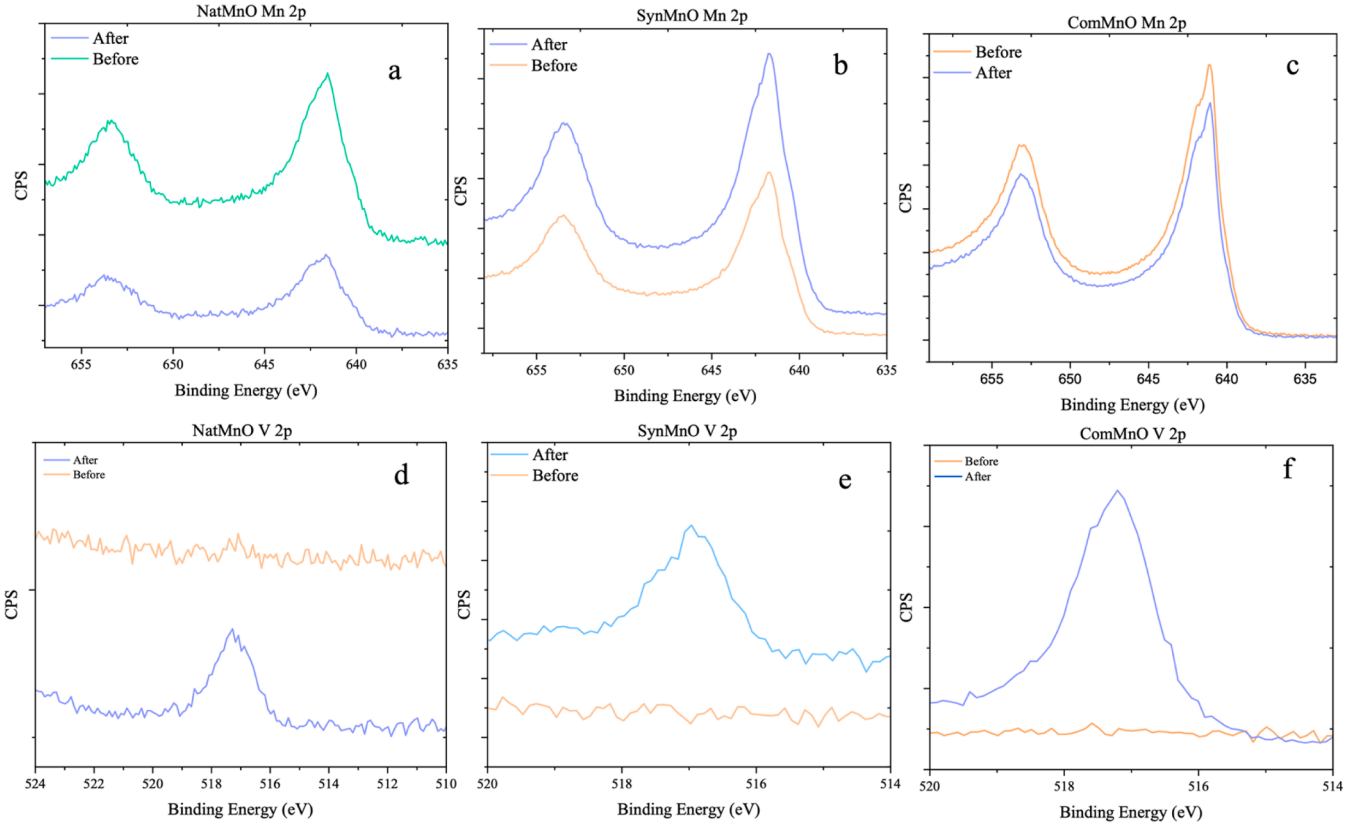

Fig. 9. XPS Mn and V spectra by XPS of MnOx. (a. NatMnO, b. SynMnO, c. ComMnO of Mn spectra; d. NatMnO, e. SynMnO, f. ComMnO of V spectra).

minor peak at approximately 517 eV, corresponding to V(V) oxide without oxidation states changes.

3.5. Stability and reusability

An effective adsorbent should not only exhibit excellent performance but also demonstrate good reusability. Regenerating an adsorbent with exhausted adsorption sites enables these sites to be reused, reducing the overall cost of adsorption technology as a water purification method. The results of the desorption experiments by washing using DIW (Fig. 10) indicated that the desorption of V by MnOx was significantly lower than its adsorption. This suggests that MnOx exhibited a strong adsorption capacity for V, and that it is difficult to desorb V using deionised water. It also corroborates the sorption isotherm data which indicate that the adsorption mechanism of V by MnOx was both physical and chemical adsorption. This is also advantageous from both environmental and process engineering perspectives, as MnOx exhibits strong binding of sorbed vanadium, minimising the risk of its release into the environment.

Fig. 11 shows the changes in V adsorption capacity of the regenerated MnOx adsorbents. The retained adsorption capacity refers to the ratio of the adsorption capacity of MnOx adsorbent after adsorption-desorption cycles to that of original MnOx adsorbents. During the initial adsorption, the adsorption capacities of MnOx were NatMnO 8.87 mg/g, SynMnO 5.50 mg/g, and ComMnO 2.58 mg/g. Following three cycles of adsorption-desorption, the maximum V adsorption capacity of MnOx reached up to 19.3 mg/g for SynMnO, 18.4 mg/g for NatMnO, and 16.7 mg/g for ComMnO. All adsorbents were reused for at least three cycles of adsorption and desorption while the adsorption capacity remained stable or increased. The increase in adsorption capacity may be due to the reaction of MnOx with the acidic V solution or agitation during the sorption experiments that resulted in a change in the physical properties of the surface [66]. Given that similar increases in adsorption capacity were observed when the MnOx were regenerated with acidic, basic and neutral solutions, it is unlikely that chemical reactions induced by the regeneration solutions contributed to the increased adsorption capacity.

Overall, the adsorption capacity of MnOx remained stable or improved after the adsorption-desorption cycle, confirming its effective regeneration and reusability for V removal. This highlights MnOx as a promising and sustainable water treatment technology for vanadium-containing waters. Manganese concentrations in the post-adsorption solution were below ICP-OES detection limit, suggesting that MnOx underwent minimal dissolution during the V adsorption and desorption process, which is consistent with its chemical insolubility in water, suggesting that its application would not result in secondary Mn contamination of wastewaters.

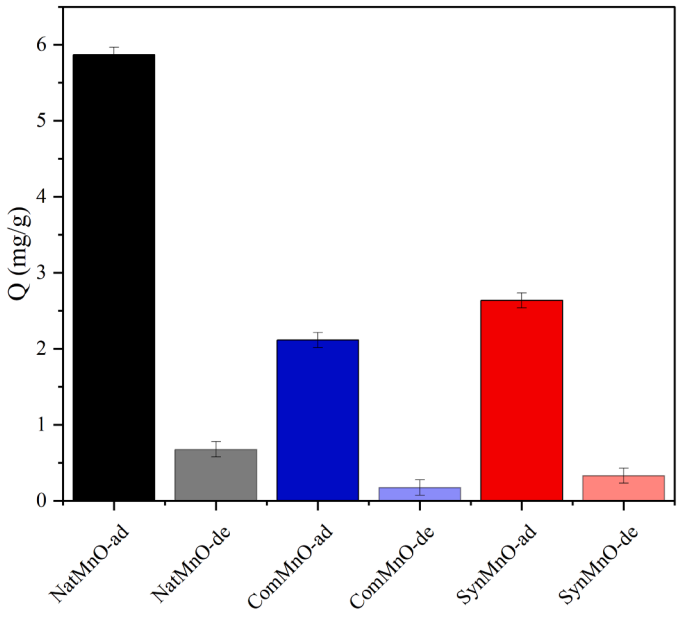

Fig. 10. V amount adsorbed and desorbed by MnOx (desorption by DIW, ad: adsorption, de: desorption).

3.6. Mechanism of V sorption onto MnOx

The adsorption mechanism of V sorption onto MnOx under acidic conditions, as evidenced using sorption isotherm data, and analytical characterisation of residues using SEM-EDS and XPS, suggest that it was a combination of physical and electrostatic adsorption. Zeta potential measurements at pH 3 suggest that MnOx species carried a negative charge (NatMnO and SynMnO), whilst V species were likely to be positively charged during such conditions.

Vanadium adsorption was determined to be highly dependent on the surface properties of MnOx and the concentration of V ions. The different V adsorption capacities exhibited by the three MnOx was likely due to a combination of their different MnO_2 structure, specific surface areas, pore sizes, pore volumes, and pH_{pzc}. Vanadium sorption was best fit using a pseudo-second-order model, suggesting that both chemisorption and physical sorption, potentially involving electron sharing or exchange, contributed to the adsorption mechanism. Alignment of data with Freundlich and Redlich-Peterson models indicate that V adsorption onto MnOx was not as a monolayer adsorption, but instead, likely to have involved a combination of chemical reaction-based adsorption (chemisorption) and multilayer adsorption mechanisms. This further validates the hypothesis that V sorption via a mixed chemical and physical process.

4. Conclusion

Optimum conditions for V adsorption on MnOx were identified to be pH 2, 0.01 M $NaNO_3$ and 2 g/L sorbent concentration. Adsorption of V by MnOx proceeded by a dual physical and chemical surface complexation which resulted in multilayer adsorption. Kinetic models and adsorption isotherms highlighted the heterogeneous nature of the MnOx surfaces, and the complex mechanisms involved in the V adsorption processes. Sorption capacity was high (54.0 mg/g exhibited by NatMnO) and the sorbents were also determined to be reusable. Crucially, this strong performance and reusability at acidic pH suggests that MnOx is highly effective and sustainable for the removal of V from a wide range of commonly occurring industrial and mining acidic waste waters. Further research could focus on optimizing regeneration techniques, upscaling the experimental design, including test sorbent efficacy in flow-through systems.

Environmental implication

Manganese oxide minerals (MnOx) can be used to remove toxic and potentially carcinogenic vanadium (V) from acidic water contaminated by mining and industrial activities. The effective adsorption of V by MnOx serves to mitigate environmental and health risks. Our results demonstrate that the MnOx can be reused multiple times, which reduces waste and lowers costs, thereby enhancing the sustainability of this water treatment processes. In conclusion, manganese oxide adsorbents represent an efficient method for the mitigation of vanadium pollution in water systems.

CRediT authorship contribution statement

Crane Richard: Writing – review & editing, Supervision, Methodology, Conceptualization. **Morgan David:** Writing – review & editing, Methodology. **Hudson-Edwards Karen A.:** Writing – review & editing.

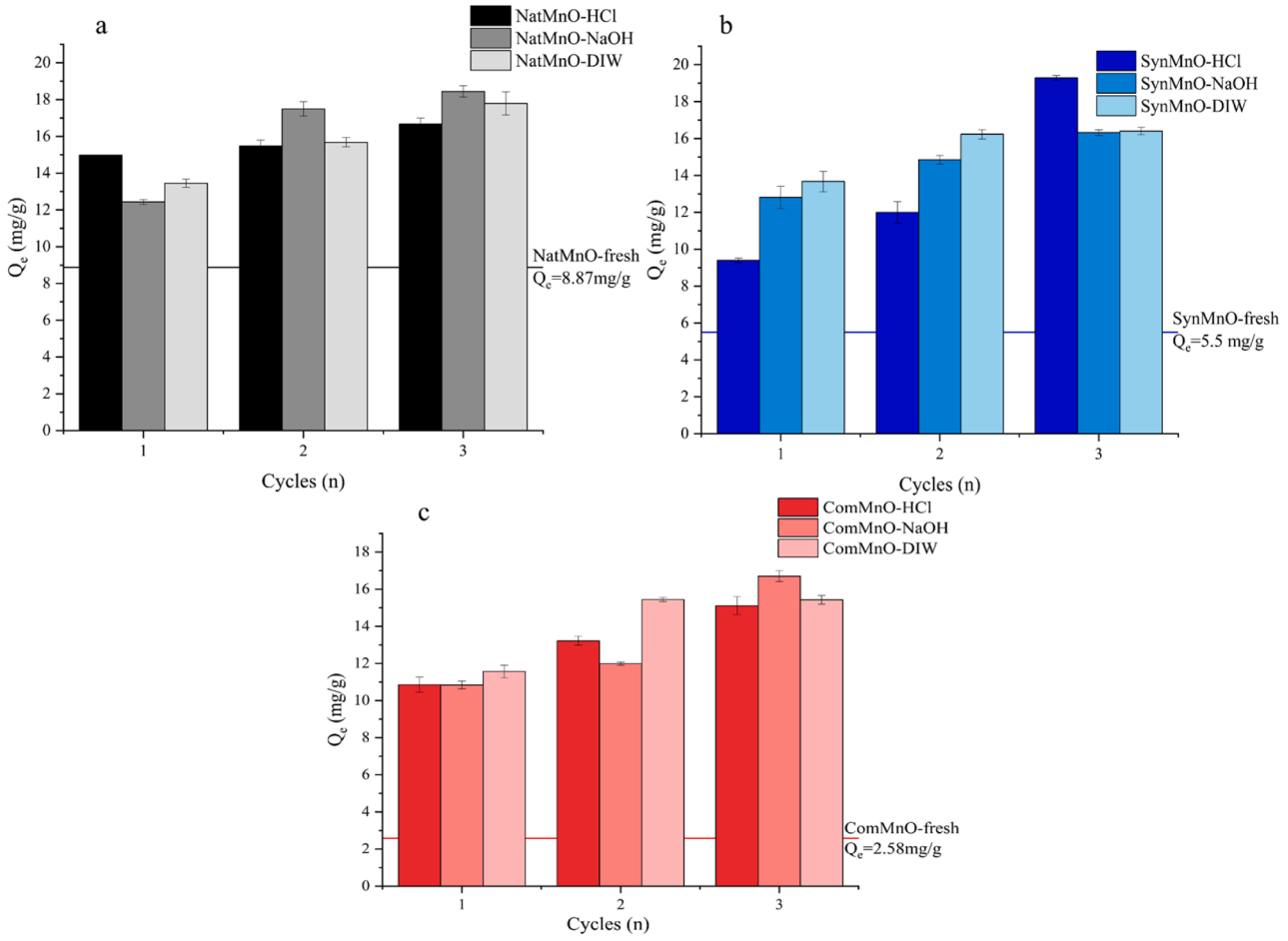

Fig. 11. V adsorption capacity of the regenerated MnOx after washing in 0.1 M HCl, 0.1 M NaOH, and DIW (a. NatMnO, b. SynMnO, c. ComMnO).

Graf Arthur: Writing – original draft, Software, Resources, Methodology. **Newsome Laura:** Writing – review & editing, Supervision, Methodology. **Li Peirou:** Writing – original draft, Visualization, Investigation, Funding acquisition, Formal analysis, Data curation, Conceptualization.

Declaration of Competing Interest

The authors declare that they have no known competing financial interests or personal relationships that could have appeared to influence the work reported in this paper.

Acknowledgement

P. L. acknowledges financial support from the University of Exeter-China Scholarship Council PhD Scholarship and the LimeTree Capital PhD China Scholarship Fund. X-ray photoelectron (XPS) data were acquired at the EPSRC National Facility for XPS ("HarwellXPS," EP/Y023587/1, EP/Y023609/1, EP/Y023536/1, EP/Y023552/1, and EP/Y023544/1). The authors would like to thank Dr. Gavyn Rollinson and Dr. Hong Chang for their contribution to the University of Exeter's XRD, SEM, TEM, and EDS equipment support, and Dr. Pierre Josso from the British Geological Survey for supplying the natural MnOx sample.

Appendix A. Supporting information

Supplementary data associated with this article can be found in the online version at doi:10.1016/j.jhazmat.2025.137765.

Data availability

The authors are unable or have chosen not to specify which data has been used.

References

[1] Aarabi-Karasgani, M., Rashchi, F., Mostoufi, N., Vahidi, E., 2010. Leaching of vanadium from LD converter slag using sulfuric acid. Hydrometallurgy 102 (1), 14–21. https://doi.org/10.1016/j.hydromet.2010.01.006.

[2] Abernathy, M.J., Schaefer, M.V., Ramirez, R., Garniwan, A., Lee, I., Zaera, F., Polizzotto, M.L., Ying, S.C., 2022. Vanadate retention by iron and manganese oxides. ACS Earth Space Chem 6 (8), 2041–2052. https://doi.org/10.1021/acsearthspacechem.2c00116.

[3] Abernathy, M.J., Schaefer, M.V., Vessey, C.J., Liu, H., Ying, S.C., 2021. Oxidation of V (IV) by birnessite: kinetics and surface complexation. Environ Sci Technol 55 (17), 11703–11712.

[4] Al Abdullah, J., Al Lafi, A.G., Al Masri, Wa, Amin, Y., Alnama, T., 2016. Adsorption of cesium, cobalt, and lead onto a synthetic nano manganese oxide: behavior and mechanism. Water, Air, Soil Pollut 227 (7), 241. https://doi.org/10.1007/s11270-016-2938-4.

[5] Ali, L.I.A., Ismail, H.K., Alesary, H.F., Aboul-Enein, H.Y., 2021. A nanocomposite based on polyaniline, nickel and manganese oxides for dye removal from aqueous solutions. Int J Environ Sci Technol 18 (7), 2031–2050. https://doi.org/10.1007/s13762-020-02961-0.

[6] Amarray, A., El Ghachtouli, S., Leroy, J., Bonnaillie, P., Khaless, K., Dahbi, M., Azzi, M., 2021. Mesoporous nanomaterials based on manganese with different interlayer alkali cations: an efficient approach for the removal of Pb(II) and Cd(II) from aqueous medium. J Water Process Eng 40, 101944. https://doi.org/10.1016/j.jwpe.2021.101944.

[7] An, B., 2020. Cu(II) and As(V) adsorption kinetic characteristic of the multifunctional amino groups in Chitosan. Processes 8 (9), 1194.

[8] An, Y., Ma, B., Li, X., Chen, Y., Wang, C., Wang, B., Gao, M., Feng, G., 2023. A review on the roasting-assisted leaching and recovery of V from vanadium slag. Process Saf Environ Prot 173, 263–276. https://doi.org/10.1016/j.psep.2023.03.013.

[9] Assem, F.L., Levy, L.S., 2012. Inhalation toxicity of vanadium. Vanadium: Biochem Mol Biol Approaches 209–224.
[10] Babaeivelni, K., Khodadoust, A.P., Bogdan, D., 2014. Adsorption and removal of arsenic (V) using crystalline manganese (II,III) oxide: kinetics, equilibrium, effect of pH and ionic strength. J Environ Sci Health, Part A 49 (13), 1462–1473. https://doi.org/10.1080/10934529.2014.937160.
[11] Bello, A., Leiviskä, T., Zhang, R., Tanskanen, J., Maziarz, P., Matusik, J., Bhatnagar, A., 2019. Synthesis of zerovalent iron from water treatment residue as a conjugate with kaolin and its application for vanadium removal. J Hazard Mater 374, 372–381. https://doi.org/10.1016/j.jhazmat.2019.04.056.
[12] Blanchard, G., Maunaye, M., Martin, G., 1984. Removal of heavy metals from waters by means of natural zeolites. Water Res 18 (12), 1501–1507.
[13] Chen, Z., Ma, W., Han, M., 2008. Biosorption of nickel and copper onto treated alga (Undaria pinnatifida): Application of isotherm and kinetic models. J Hazard Mater 155 (1), 327–333. https://doi.org/10.1016/j.jhazmat.2007.11.064.
[14] Chiam, S.-L., Pung, S.-Y., Yeoh, F.Y., Ahmadipour, M., 2022. Highly efficient oxidative degradation of organic dyes by manganese dioxide nanoflowers. Mater Chem Phys 280, 125848. https://doi.org/10.1016/j.matchemphys.2022.125848.
[15] Dakroury, G.A., El-Shazly, E.A.A., Eliwa, A.A., Mubark, A.E., El-Azony, K.M., 2022. Utilization of titanium nanocomposites as prospective materials for recycling of vanadium (V) from waste solutions. J Mol Liq 366, 120170. https://doi.org/10.1016/j.molliq.2022.120170.
[16] Della Puppa, L., Komárek, M., Bordas, F., Bollinger, J.-C., Joussein, E., 2013. Adsorption of copper, cadmium, lead and zinc onto a synthetic manganese oxide. J Colloid Interface Sci 399, 99–106. https://doi.org/10.1016/j.jcis.2013.02.029.
[17] Fairley, N., Fernandez, V., Richard-Plouet, M., Guillot-Deudon, C., Walton, J., Smith, E., Flahaut, D., Greiner, M., Biesinger, M., Tougaard, S., Morgan, D., Baltrusaitis, J., 2021. Systematic and collaborative approach to problem solving using X-ray photoelectron spectroscopy. Appl Surf Sci Adv 5, 100112. https://doi.org/10.1016/j.apsadv.2021.100112.
[18] Gan, C., Liu, M., Lu, J., Yang, J., 2020. Adsorption and desorption characteristics of vanadium (V) on silica. Water, Air, Soil Pollut 231 (1), 10. https://doi.org/10.1007/s11270-019-4377-5.
[19] Ghanim, B., Murnane, J.G., O'Donoghue, L., Courtney, R., Pembroke, J.T., O'Dwyer, T.F., 2020. Removal of vanadium from aqueous solution using a red mud modified saw dust biochar. J Water Process Eng 33, 101076. https://doi.org/10.1016/j.jwpe.2019.101076.
[20] Gogoi, H., Zhang, R., Matusik, J., Leiviskä, T., Rämö, J., Tanskanen, J., 2021. Vanadium removal by cationized sawdust produced through iodomethane quaternization of triethanolamine grafted raw material. Chemosphere 278, 130445. https://doi.org/10.1016/j.chemosphere.2021.130445.
[21] Gouy, M., 1910. Sur la constitution de la charge électrique à la surface d'un électrolyte. J Phys Theor Appl 9 (1), 457–468.
[22] Guo, Y., Li, H.-Y., Shen, S., Cheng, J., Diao, J., Xie, B., 2021. A novel process for comprehensive resource utilization of hazardous chromium sludge: progressive recovery of Si, V, Fe and Cr. J Hazard Mater 405, 124669. https://doi.org/10.1016/j.jhazmat.2020.124669.
[23] Gypser, S., Hirsch, F., Schleicher, A.M., Freese, D., 2018. Impact of crystalline and amorphous iron- and aluminum hydroxides on mechanisms of phosphate adsorption and desorption. J Environ Sci 70, 175–189. https://doi.org/10.1016/j.jes.2017.12.001.
[24] Hu, X., Zhang, Q., Yu, Y., Hu, Y., Wang, Y., 2020. Removal of Zr(IV) from aqueous solution using hydrated manganese oxide derived from the modified Hummers method. Chem Phys Lett 752, 137585. https://doi.org/10.1016/j.cplett.2020.137585.
[25] Huang, J., Fan, Y., Liu, T., Zhang, Y., Hu, P., 2023. Carbon capture technology exploitation for vanadium tailings and assessment of CO2 sequestration potential. J Environ Manag 331, 117338. https://doi.org/10.1016/j.jenvman.2023.117338.
[26] Huang, Q., Xiang, J., Wang, X., Pei, G., Lv, X., 2020. Dissolution kinetics of calcium vanadates in sulfuric acid: a fundamental study for the vanadium extraction process. J Chem Technol Biotechnol 95 (6), 1773–1780.
[27] Huang, X., Chen, T., Zou, X., Zhu, M., Chen, D., Pan, M., 2017. The adsorption of Cd (II) on manganese oxide investigated by batch and modeling techniques. Int J Environ Res Public Health 14 (10), 1145.
[28] Jegadeesan, G., Al-Abed, S.R., Sundaram, V., Choi, H., Scheckel, K.G., Dionysiou, D.D., 2010. Arsenic sorption on TiO2 nanoparticles: size and crystallinity effects. Water Res 44 (3), 965–973. https://doi.org/10.1016/j.watres.2009.10.047.
[29] Jiang, Y., Yin, X., Luo, X., Yu, L., Sun, H., Wang, N., Mathews, S., 2019. Sorption of vanadium (V) on three typical agricultural soil of the Loess Plateau, China. Environ Pollut Bioavailab 31 (1), 120–130. https://doi.org/10.1080/26395940.2019.1590162.
[30] Kalam, S., Abu-Khamsin, S.A., Kamal, M.S., Patil, S., 2021. Surfactant adsorption isotherms: a review. ACS Omega 6 (48), 32342–32348. https://doi.org/10.1021/acsomega.1c04661.
[31] Kończyk, J., Kluziak, K., Kołodyńska, D., 2022. Adsorption of vanadium (V) ions from the aqueous solutions on different biomass-derived biochars. J Environ Manag 313, 114958. https://doi.org/10.1016/j.jenvman.2022.114958.
[32] Lagergren, S., 1898. About the theory of so-called adsorption of soluble substances.
[33] Lee, J.-c, Kurniawan, Kim, E.-y, Chung, K.W., Kim, R., Jeon, H.-S., 2021. A review on the metallurgical recycling of vanadium from slags: towards a sustainable vanadium production. J Mater Res Technol 12, 343–364. https://doi.org/10.1016/j.jmrt.2021.02.065.
[34] Leiviskä, T., 2021. Chapter 21 - Vanadium(V) removal from water by sorption. In: Núñez-Delgado, A. (Ed.), Sorbents Materials for Controlling Environmental Pollution. Elsevier, pp. 543–571. https://doi.org/10.1016/B978-0-12-820042-1.00008-0.
[35] Li, H., Han, K., Shang, J., Cai, W., Pan, M., Xu, D., Du, C., Zuo, R., 2022. Comparison of adsorption capacity and removal efficiency of strontium by six typical adsorption materials. Sustainability 14 (13), 7723.
[36] Li, H., Huang, Y., Luo, Q., Liu, J., 2022. The simultaneous reduction and adsorption for V(V) and Cr(VI) anionic species in aqueous solution by polyethyleneimine cross-linked titanate nanotubes. Sep Purif Technol 299, 121682. https://doi.org/10.1016/j.seppur.2022.121682.
[37] Li, J., Zhang, Y., Du, D., Liu, Z., 2017. Improvements in the decision making for cleaner production by data mining: case study of vanadium extraction industry using weak acid leaching process. J Clean Prod 143, 582–597. https://doi.org/10.1016/j.jclepro.2016.12.071.
[38] Li, P., Deng, S., Wu, Y., Li, S., Huangfu, Z., Sun, X., Yu, J., 2022. Effect of humin modified by Fe(NO3)3/FeSO4 on the bioavailability of vanadium in Panzhihua mining: characteristics and mechanisms. Environ Earth Sci 82 (1), 8. https://doi.org/10.1007/s12665-022-10685-2.
[39] Liu, J., Huang, Y., Li, H., Duan, H., 2022. Recent advances in removal techniques of vanadium from water: a comprehensive review. Chemosphere 287, 132021. https://doi.org/10.1016/j.chemosphere.2021.132021.
[40] Loganathan, P., Burau, R., Fuerstenau, D., 1977. Influence of pH on the sorption of Co^{2+}, Zn^{2+} and Ca^{2+} by a hydrous manganese oxide. Soil Sci Soc Am J 41 (1), 57–62.
[41] Low, M., 1960. Kinetics of chemisorption of gases on solids. Chem Rev 60 (3), 267–312.
[42] Luo, X., Yu, L., Wang, C., Yin, X., Mosa, A., Lv, J., Sun, H., 2017. Sorption of vanadium (V) onto natural soil colloids under various solution pH and ionic strength conditions. Chemosphere 169, 609–617. https://doi.org/10.1016/j.chemosphere.2016.11.105.
[43] Manohar, D.M., Noeline, B.F., Anirudhan, T.S., 2005. Removal of Vanadium(IV) from aqueous solutions by adsorption process with aluminum-pillared bentonite. Ind Eng Chem Res 44 (17), 6676–6684. https://doi.org/10.1021/ie0490841.
[44] Mazurek, K., 2013. Recovery of vanadium, potassium and iron from a spent vanadium catalyst by oxalic acid solution leaching, precipitation and ion exchange processes. Hydrometallurgy 134-135, 26–31. https://doi.org/10.1016/j.hydromet.2013.01.011.
[45] Moskalyk, R.R., Alfantazi, A.M., 2003. Processing of vanadium: a review. Miner Eng 16 (9), 793–805. https://doi.org/10.1016/S0892-6875(03)00213-9.
[46] Musil, M., Choi, B., Tsutsumi, A., 2015. Morphology and electrochemical properties of α-, β-, γ-, and δ-MnO2 synthesized by redox method. J Electrochem Soc 162 (10), A2058.
[47] Naeem, A., Westerhoff, P., Mustafa, S., 2007. Vanadium removal by metal (hydr) oxide adsorbents. Water Res 41 (7), 1596–1602. https://doi.org/10.1016/j.watres.2007.01.002.
[48] Omidinasab, M., Rahbar, N., Ahmadi, M., Kakavandi, B., Ghanbari, F., Kyzas, G.Z., Martinez, S.S., Jaafarzadeh, N., 2018. Removal of vanadium and palladium ions by adsorption onto magnetic chitosan nanoparticles. Environ Sci Pollut Res 25, 34262–34276.
[49] Peng, D.-Y., Robinson, D.B., 1976. A new two-constant equation of state. Ind Eng Chem Fundam 15 (1), 59–64. https://doi.org/10.1021/i160057a011.
[50] Program, N.T., 2002. Toxicology and Carcinogenesis Studies of Vanadium Pentoxide (CAS No. 1314-62-1) in F344/N Rats and B6C3F1 Mice (Inhalation Studies). US Department of Health and Human Services, Public Health Service, National Insitutes of Health, Research Triangle Park, NC, NTP Technical Report (507).
[51] Pullin, H., Crane, R.A., Morgan, D.J., Scott, T.B., 2017. The effect of common groundwater anions on the aqueous corrosion of zero-valent iron nanoparticles and associated removal of aqueous copper and zinc. J Environ Chem Eng 5 (1), 1166–1173. https://doi.org/10.1016/j.jece.2017.01.038.
[52] Qin, Z., Wang, Y., Sun, L., Gu, Y., Zhao, Y., Xia, L., Liu, Y., Van der Bruggen, B., Zhang, Y., 2022. Vanadium recovery by electrodialysis using polymer inclusion membranes. J Hazard Mater 436, 129315. https://doi.org/10.1016/j.jhazmat.2022.129315.
[53] Rani, N., Goswami, B., Vats, R., Jangra, N., Bhukkal, C., Ahlawat, R., 2023. Multiphase manganese oxide nanoparticles suitable for optical and catalytic applications. Mater Today: Proc. https://doi.org/10.1016/j.matpr.2023.03.158.
[54] Rehder, D., 2016. Perspectives for vanadium in health issues. Future Med Chem 8 (3), 325–338.
[55] Roy, A., Chakraborty, S., Kundu, S.P., Adhikari, B., Majumder, S., 2012. Adsorption of anionic-azo dye from aqueous solution by lignocellulose-biomass jute fiber: equilibrium, kinetics, and thermodynamics study. Ind Eng Chem Res 51 (37), 12095–12106.
[56] Saeed, T., Naeem, A., Mahmood, T., Ahmad, Z., Farooq, M., Farida, Din, I.U., Khan, I.W., 2021. Comparative study for removal of cationic dye from aqueous solutions by manganese oxide and manganese oxide composite. Int J Environ Sci Technol 18 (3), 659–672. https://doi.org/10.1007/s13762-020-02844-4.
[57] Schindler, M., Hawthorne, F.C., Baur, W.H., 2000. A crystal-chemical approach to the composition and occurrence of vanadium minerals. Can Mineral 38 (6), 1443–1456. https://doi.org/10.2113/gscanmin.38.6.1443.
[58] Ścibior, A., Pietrzyk, Ł., Plewa, Z., Skiba, A., 2020. Vanadium: risks and possible benefits in the light of a comprehensive overview of its pharmacotoxicological mechanisms and multi-applications with a summary of further research trends. J Trace Elem Med Biol 61, 126508. https://doi.org/10.1016/j.jtemb.2020.126508.
[59] Scott, T.B., Popescu, I.C., Crane, R.A., Noubactep, C., 2011. Nano-scale metallic iron for the treatment of solutions containing multiple inorganic contaminants.

J Hazard Mater 186 (1), 280–287. https://doi.org/10.1016/j.jhazmat.2010.10.113.
[60] Sedgwick, P., 2012. Pearson's correlation coefficient. Bmj 345.
[61] Sharififard, H., Zokaee Ashtiani, F., Soleimani, M., 2013. Adsorption of palladium and platinum from aqueous solutions by chitosan and activated carbon coated with chitosan. Asia-Pac J Chem Eng 8 (3), 384–395.
[62] Song, H., Yang, G., Song, H., Cui, X., Li, F., Yuan, D., 2016. Kinetic and thermodynamic studies on adsorption of thiophene and benzothiophene onto AgCeY Zeolite. J Taiwan Inst Chem Eng 63, 125–132.
[63] Stanisz, M., Klapiszewski, Ł., Kołodyńska, D., Jesionowski, T., 2021. Development of functional lignin-based spherical particles for the removal of vanadium(V) from an aqueous system. Int J Biol Macromol 186, 181–193. https://doi.org/10.1016/j.ijbiomac.2021.07.046.
[64] Suib, S.L., 2017. A review of recent developments of mesoporous materials. Chem Rec 17 (12), 1169–1183.
[65] Tebo, B.M., Clement, B.G., Dick, G.J., 2007. Biotransformations of manganese. Man Environ Microbiol 1223–1238.
[66] Vakili, M., Deng, S., Cagnetta, G., Wang, W., Meng, P., Liu, D., Yu, G., 2019. Regeneration of chitosan-based adsorbents used in heavy metal adsorption: a review. Sep Purif Technol 224, 373–387. https://doi.org/10.1016/j.seppur.2019.05.040.
[67] Vasseghian, Y., Sadeghi Rad, S., Vilas–Boas, J.A., Khataee, A., 2021. A global systematic review, meta-analysis, and risk assessment of the concentration of vanadium in drinking water resources. Chemosphere 267, 128904. https://doi.org/10.1016/j.chemosphere.2020.128904.
[68] Waidyanatha, S., Weber, F.X., Fallacara, D.M., Harrington, J.M., Levine, K., Robinson, V.G., Sparrow, B.R., Stout, M.D., Fernando, R., Hooth, M.J., Xie, G., Roberts, G.K., 2022. Systemic exposure and urinary excretion of vanadium following perinatal subchronic exposure to vanadyl sulfate and sodium metavanadate via drinking water. Toxicol Lett 360, 53–61. https://doi.org/10.1016/j.toxlet.2022.03.004.
[69] Wang, H., Lv, Z., Song, Y., Wang, Y.-n, Zhang, D., Sun, Y., Tsang, Y.F., Pan, X., 2019. Adsorptive removal of Sb(III) from wastewater by environmentally-friendly biogenic manganese oxide (BMO) materials: Efficiency and mechanisms. Process Saf Environ Prot 124, 223–230. https://doi.org/10.1016/j.psep.2019.02.022.
[70] Wen, J., Sun, Y., Ning, P., Xu, G., Sun, S., Sun, Z., Cao, H., 2022. Deep understanding of sustainable vanadium recovery from chrome vanadium slag: promotive action of competitive chromium species for vanadium solvent extraction. J Hazard Mater 422, 126791. https://doi.org/10.1016/j.jhazmat.2021.126791.
[71] Wu, B., Ifthikar, J., Oyekunle, D.T., Jawad, A., Chen, Z., Chen, Z., Sellaoui, L., Bouzid, M., 2021. Interpret the elimination behaviors of lead and vanadium from the water by employing functionalized biochars in diverse environmental conditions. Sci Total Environ 789, 148031. https://doi.org/10.1016/j.scitotenv.2021.148031.
[72] Xiang, J., Huang, Q., Lv, X., Bai, C., 2018. Extraction of vanadium from converter slag by two-step sulfuric acid leaching process. J Clean Prod 170, 1089–1101. https://doi.org/10.1016/j.jclepro.2017.09.255.
[73] Xu, X., Gao, B., Jin, B., Yue, Q., 2016. Removal of anionic pollutants from liquids by biomass materials: a review. J Mol Liq 215, 565–595. https://doi.org/10.1016/j.molliq.2015.12.101.
[74] Yadav, G.G., Wei, X., Gallaway, J.W., Chaudhry, Z., Shin, A., Huang, J., Yakobov, R., Nyce, M., Vanderklaauw, N., Banerjee, S., 2017. Rapid electrochemical synthesis of δ-MnO_2 from γ-MnO_2 and unleashing its performance as an energy dense electrode. Mater Today Energy 6, 198–210. https://doi.org/10.1016/j.mtener.2017.10.008.
[75] Yang, J., Teng, Y., Wu, J., Chen, H., Wang, G., Song, L., Yue, W., Zuo, R., Zhai, Y., 2017. Current status and associated human health risk of vanadium in soil in China. Chemosphere 171, 635–643. https://doi.org/10.1016/j.chemosphere.2016.12.058.
[76] Yang, J.-y, Luo, H.-q, Zhu, Y.-y, Yu, Y.-q, He, W.-y, Wu, Z.-z, Wang, B., 2020. Adsorption-desorption and co-migration of vanadium on colloidal kaolinite. Environ Sci Pollut Res 27 (15), 17910–17922. https://doi.org/10.1007/s11356-020-07845-x.
[77] Yang, R., Fan, Y., Ye, R., Tang, Y., Cao, X., Yin, Z., Zeng, Z., 2021. MnO2-based materials for environmental applications. Adv Mater 33 (9), 2004862. https://doi.org/10.1002/adma.202004862.
[78] Yin, X., Yu, L., Luo, X., Zhang, Z., Sun, H., Mosa, A.A., Wang, N., 2019. Sorption of Pb (II) onto < 1 μm effective diameter clay minerals extracted from different soils of the Loess Plateau, China. Geoderma 337, 1058–1066. https://doi.org/10.1016/j.geoderma.2018.11.027.
[79] Yu, J., Ma, B., Zhao, S., Yao, Z., Wang, C., Wang, B., Gao, M., Feng, G., 2023. Vanadium extraction from water-cooled vanadium converter slag via salt-free roasting and acid leaching. Process Saf Environ Prot 172, 727–737. https://doi.org/10.1016/j.psep.2023.02.071.
[80] Zhang, H., Wu, A., Fu, H., Zhang, L., Liu, H., Zheng, S., Wan, H., Xu, Z., 2017. Efficient removal of Pb (II) ions using manganese oxides: the role of crystal structure. RSC Adv 7 (65), 41228–41240.
[81] Zhang, L., Wang, J., Qiao, H., Liu, F., Fu, Z., 2020. Synthesis of manganese oxides for adsorptive removal of ammonia nitrogen from aqueous solutions. J Clean Prod 272, 123055. https://doi.org/10.1016/j.jclepro.2020.123055.
[82] Zhang, R., Zhang, B., Leiviskä, T., 2022. Vanadium recovery from spent iron sorbent used for the treatment of mining-influenced water. Resour, Conserv Recycl 182, 106291. https://doi.org/10.1016/j.resconrec.2022.106291.
[83] Zhu, H., Xiao, X., Guo, Z., Han, X., Liang, Y., Zhang, Y., Zhou, C., 2018. Adsorption of vanadium (V) on natural kaolinite and montmorillonite: characteristics and mechanism. Appl Clay Sci 161, 310–316. https://doi.org/10.1016/j.clay.2018.04.035.
[84] Zhu, H., Xiao, X., Guo, Z., Peng, C., Wang, X., Yang, A., 2020. Characteristics and behaviour of vanadium (V) adsorption on goethite and birnessite. Environ Earth Sci 79 (10), 1.
[85] Zhu, X., Yang, X., Li, W., Liu, Y., 2022. Efficient removal and recovery of vanadium (IV and V) from high acidic waste water with resins D851 and D201: a comparative study. J Water Process Eng 49, 103153. https://doi.org/10.1016/j.jwpe.2022.103153.
[86] Zhu, X., Zhou, Z., Jin, J., Li, Y., Han, Y., 2023. Vanadium extraction from V-bearing shale using oxidation roasting and acid leaching. Miner Eng 192, 107985. https://doi.org/10.1016/j.mineng.2022.107985.